A Concatenated Dual Displacement Code for Continuous-Variable Quantum Error Correction

Fucheng Guo [*] and Frank Mueller [†]
Department of Computer Science, North Carolina State University, Raleigh, North Carolina 27695-8206, USA

Yuan Liu [‡]
Department of Electrical and Computer Engineering, North Carolina State University, Raleigh, North Carolina 27695, USA
Department of Computer Science, North Carolina State University, Raleigh, North Carolina 27695, USA and
Department of Physics, North Carolina State University, Raleigh, North Carolina 27695, USA

(Dated: May 12, 2026)

The continuous-variable (CV) Gaussian no-go theorem fundamentally limits the suppression of Gaussian displacement errors using only Gaussian gates and states. Prior studies have employed Gottesman–Kitaev–Preskill (GKP) states as ancillary qumodes to suppress small Gaussian displacement errors. However, when the displacement magnitude becomes large, inevitable lattice-crossing errors arise beyond the correctable range of the GKP state. To address this issue, we concatenate the Gaussian-noise-suppression circuit with an outer analog Steane code that corrects such occasional lattice-crossing events as well as other abrupt displacement errors. Contrary to conventional concatenation, which primarily aims to reduce logical error rates, the Steane–GKP duality in encoding provides complementary protection against both large and small displacement errors. In fact, it is precisely this combination that makes CV error correction possible. In contrast to prior work on concatenating GKP and repetition codes to establish error correction for discrete qubit/qudit encoding, we provide correction in the continuous encoding space. Analytical studies show that, under infinite squeezing, the concatenated code suppresses the variance of Gaussian displacement errors acting on all qumodes by up to 50%, while enabling unbiased correction of lattice-crossing errors with a success probability determined by the ratio between the residual Gaussian error standard deviation and the lattice-crossing magnitude. Even with finite squeezing, the proposed architecture still provides Gaussian-error suppression and lattice-crossing correction. Moreover, the presence of the outer analog Steane code relaxes the squeezing requirement of the inner GKP states, indicating near-term experimental feasibility. This work establishes a viable route toward fault-tolerant continuous-variable quantum computation and provides insight into the design of concatenated CV error-correcting architectures.

CONTENTS

I. INTRODUCTION

Quantum error correction (QEC) lies at the foundation of fault-tolerant quantum computation, enabling reliable information processing in the presence of noise and decoherence [1–3]. In addition to qubit-based schemes, bosonic quantum error correction encodes logical information into CV modes of harmonic oscillators, providing a hardware-efficient means to protect against com-

* fguo22@ncsu.edu
† fmuelle@ncsu.edu
‡ q_yuanliu@ncsu.edu

mon bosonic errors such as photon loss and displacement errors [4]. While discrete-variable (DV) qubit systems have achieved remarkable progress with stabilizer-based codes [5–7], including advanced concatenation schemes that combine GKP states with DV repetition or outer stabilizer codes to enhance error correction and approach fault-tolerant operation [8, 9], such architectures fundamentally encode logical information in discrete degrees of freedom and rely on projective syndrome extraction and digital correction mechanisms. In contrast, CV quantum architectures, such as optical modes and superconducting resonators, intrinsically encode information in continuous quadrature variables, leading to distinct error models dominated by Gaussian displacement noise and requiring analog error correction strategies beyond conventional stabilizer formalisms. These CV systems offer an attractive alternative owing to their larger Hilbert space, natural compatibility with bosonic hardware, and the possibility of leveraging phase-space structure for encoding and noise suppression [10–12]. However, the dominant errors in CV platforms take the form of Gaussian displacement noise, which cannot be fully suppressed using Gaussian operations and states alone due to the fundamental constraint of the Gaussian no-go theorem [13, 14]. Overcoming this limitation is essential for realizing scalable, fault-tolerant CV quantum computation.

A variety of theoretical frameworks have been proposed to suppress Gaussian displacement noise in continuous-variable systems that directly encode continuous logical information rather than discrete qubits [15]. Among these, GKP-type encodings occupy a central position, embedding quantum information into a lattice structure in phase space such that small displacements can be detected and corrected through modular measurements [16, 17]. Their correction capability, however, is intrinsically bounded: When the displacement magnitude exceeds half of the lattice spacing, lattice-crossing errors arise and cause logical misidentification [18, 19]. In addition, repetition-type encodings have been explored to redundantly distribute quantum information across multiple bosonic modes. Published results include several canonical examples, such as five- [20] and nine-wave-packet [21] codes, which illustrate how continuous logical variables can, in principle, be encoded with redundancy to protect against local displacement errors. Nevertheless, these repetition-based constructions remain ineffective against correlated Gaussian noise acting collectively on all qumodes, as indicated by the Gaussian no-go theorem [13]. Furthermore, they largely remain theoretical constructs, as explicit realizations of logical operations and syndrome-extraction mechanisms [22] within the encoded Hilbert space have yet to be developed.

In this work, we propose a concatenated CV error-correction architecture that integrates an outer analog Steane code (in Sec. II) with an inner GKP-assisted noise-suppression circuit (in Sec. III). Our dual approach combines two error correction methods: At the inner layer Gaussian displacement noise across all qumodes is continuously suppressed, and at the outer layer lattice-crossing and abrupt displacement errors are corrected as they occasionally exceed the GKP correction range. Beyond establishing the concatenated structure, a complete operational framework is contributed for the analog Steane code by explicitly formulating its logical operations and syndrome-extraction mechanisms within the encoded Hilbert space in Sec. II. Through theoretical analysis in Sec. IV, the error-suppression capability of the concatenated code [23] is evaluated, the lower bound of achievable noise reduction is derived, and the experimental feasibility of the proposed architecture is discussed. Meanwhile, Sec. IV presents Monte Carlo simulation results, which provide a direct illustration of the performance of the concatenated code. These results provide important theoretical implications for developing scalable and fault-tolerant CV quantum information processing [24]. Sec. V concludes the paper.

II. ANALOG STEANE CODE

In this section, an analog version of the Steane code is constructed based on its DV counterpart [25]. The corresponding syndrome-extraction circuits are designed, and the implementation of fundamental logical operations is discussed. It is rigorously shown that the proposed analog Steane code can correct single-qumode displacement errors.

A. Encoding circuit

First, starting from the DV Steane code shown in Fig. 1(a), the Hadamard (H) and controlled-NOT (CNOT) gates are respectively replaced by the Fourier (F) gates and the SUM (or SUM†) gates [26]. This substitution yields the CV counterpart of the Steane code, as illustrated in Fig. 1(b). Here, The first qumode serves as the logical qumode, and $|x=0\rangle$ denotes that, in the ideal case, each qumode is initialized in a position eigenstate, whereas in practice it corresponds to a finitely squeezed vacuum state [27].

To analyze the structure of the encoded state, the Fourier gate in the position-quadrature representation is expressed as [28]

$$\hat{\mathcal{F}}\,|x\rangle \;=\; \frac{1}{\sqrt{\pi}}\int dy\, e^{2ixy}\,|y\rangle\,, \tag{1}$$

where both x and y are variables in the position basis. Only the encoding structure in the position quadrature is analyzed, since the momentum quadrature is conjugate to the position one. Therefore, the corresponding structure in the momentum quadrature can be readily obtained via a Fourier transformation and is not discussed further in this paper.

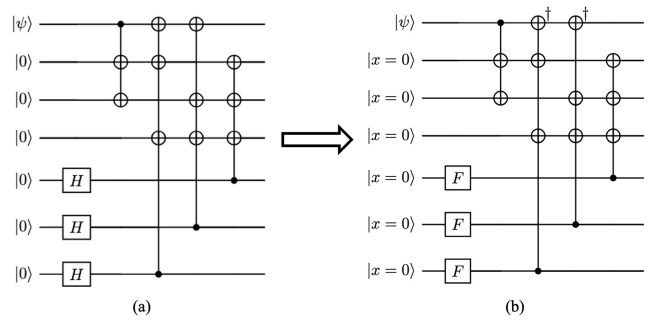

FIG. 1. (a) DV Steane code. (b) Analog Steane code obtained by replacing the H and CNOT gates with F and SUM (or SUM†) gates.

Similarly, the SUM gate in the position quadrature can be expressed as [29]

$$\mathrm{SUM}\,|x_1, x_2\rangle \;=\; |x_1,\, x_1 + x_2\rangle\,, \tag{2a}$$

$$\mathrm{SUM}^\dagger\,|x_1, x_2\rangle \;=\; |x_1,\, x_2 - x_1\rangle\,, \tag{2b}$$

where both x_1 and x_2 are variables in the position basis. The variable x_1 corresponds to the control qumode, while x_2 represents the target qumode. Based on the action of the Fourier and SUM gates, the structure of the encoded state in the position quadrature can be obtained as

$$\begin{aligned}|x_{\text{encoding}}\rangle \;=\; \frac{1}{\pi^{1.5}} \int dw\, dy\, dz\; &|x - y - z\rangle\, |x + w + z\rangle \\ &\times\; |x + w + y\rangle\, |w + y + z\rangle\, |w\rangle\, |y\rangle\, |z\rangle\end{aligned} \tag{3}$$

where x represents the encoded logical information, while w, y, and z are new variables in the position basis generated through the action of the Fourier gates.

To demonstrate that the proposed encoding structure possesses error-correcting capability, it is necessary to show that it satisfies the Knill-Laflamme condition [30, 31], i.e.,

$$\langle x'_{\text{encoding}}|\, \hat{\mathcal{E}}_\alpha^\dagger \hat{\mathcal{E}}_\beta\, |x_{\text{encoding}}\rangle \;=\; \delta(x' - x)\, \lambda_{\alpha\beta}, \quad \forall\, \alpha, \beta \tag{4}$$

where $|x_{\text{encoding}}\rangle$ and $|x'_{\text{encoding}}\rangle$ denote two different encoded states, while $\hat{\mathcal{E}}_\beta$ represents a correctable displacement error acting on the βth qumode. The coefficient $\lambda_{\alpha\beta}$ is a complex constant independent of the encoded states. This condition indicates that correctable errors do not affect the orthogonality between distinct encoded states. For example, when errors occur on qumode 1 and qumode 2 in the two encoded subspaces, we have

$$\begin{aligned}&\langle x'_{\text{encoding}}|\, \hat{\mathcal{E}}_1^\dagger \hat{\mathcal{E}}_2\, |x_{\text{encoding}}\rangle \\ &= \frac{1}{\pi^3} \int dw'\, dy'\, dz'\, dw\, dy\, dz\; \langle x' - y' - z'|\, \hat{\mathcal{E}}_1^\dagger\, |x - y - z\rangle \\ &\quad \times \langle x' + w' + z'|\, \hat{\mathcal{E}}_2\, |x + w + z\rangle \\ &\quad \times \delta(x' + w' + y' - x - w - y) \\ &\quad \times \delta(w' + y' + z' - w - y - z) \\ &\quad \times \delta(w' - w)\, \delta(y' - y)\, \delta(z' - z) \\ &= \frac{1}{\pi^3}\, \delta(x' - x)\; \langle x'|\, \hat{\mathcal{E}}_1^\dagger\, |x\rangle\; \langle x'|\, \hat{\mathcal{E}}_2\, |x\rangle\,.\end{aligned} \tag{5}$$

It can be seen that the above expression is nonzero if and only if $x = x'$. This indicates that the present encoding scheme can distinguish errors occurring on qumode 1 and qumode 2. Similarly, it can be shown that errors acting on any pair of distinct qumodes within the encoded space are distinguishable.

By expressing the encoded space in terms of the position and momentum operators, we can express it as a system of equation per qumode

$$\begin{aligned}
\text{qumode1:}\quad & \hat{x}_1^{(\text{enc})} = -\hat{p}_6 - \hat{p}_7 + \hat{x}_1, \\
& \hat{p}_1^{(\text{enc})} = \hat{p}_1 - \hat{p}_2 - \hat{p}_3, \\
\text{qumode2:}\quad & \hat{x}_2^{(\text{enc})} = \hat{p}_5 + \hat{p}_7 + \hat{x}_1 + \hat{x}_2, \\
& \hat{p}_2^{(\text{enc})} = \hat{p}_2, \\
\text{qumode3:}\quad & \hat{x}_3^{(\text{enc})} = \hat{p}_5 + \hat{p}_6 + \hat{x}_1 + \hat{x}_3, \\
& \hat{p}_3^{(\text{enc})} = \hat{p}_3, \\
\text{qumode4:}\quad & \hat{x}_4^{(\text{enc})} = \hat{p}_5 + \hat{p}_6 + \hat{p}_7 + \hat{x}_4, \\
& \hat{p}_4^{(\text{enc})} = \hat{p}_4, \\
\text{qumode5:}\quad & \hat{x}_5^{(\text{enc})} = \hat{p}_5, \\
& \hat{p}_5^{(\text{enc})} = -\hat{p}_2 - \hat{p}_3 - \hat{p}_4 - \hat{x}_5, \\
\text{qumode6:}\quad & \hat{x}_6^{(\text{enc})} = \hat{p}_6, \\
& \hat{p}_6^{(\text{enc})} = \hat{p}_1 - \hat{p}_2 - 2\hat{p}_3 - \hat{p}_4 - \hat{x}_6, \\
\text{qumode7:}\quad & \hat{x}_7^{(\text{enc})} = \hat{p}_7, \\
& \hat{p}_7^{(\text{enc})} = \hat{p}_1 - 2\hat{p}_2 - \hat{p}_3 - \hat{p}_4 - \hat{x}_7,
\end{aligned} \tag{6}$$

where $\hat{x}^{(\text{enc})}$ and $\hat{p}^{(\text{enc})}$ denote the position and momentum operators after encoding, while all other operators correspond to those in the initial state. The logical information is encoded in the first mode, whose quadrature operators $\hat{x}_1$ and $\hat{p}_1$ represent the logical position and momentum, respectively.

B. Syndrome Extraction and Error Correction

As previously demonstrated, the encoding circuit provides sufficient redundancy to distinguish displacement errors occurring on different qumodes. Next, it is necessary to design a circuit that extracts the syndrome and, based on the measurement outcomes, identifies and corrects the corresponding errors [32, 33].

The circuit shown in Fig. 2 corresponds to the position and momentum quadratures syndrome extraction circuits. For each circuit, three ancilla qumodes are introduced, each initialized in a position or momentum

eigenstate. These ancillae are coupled to the qumodes in the encoded space through a sequence of SUM or SUM† gates. Subsequently, homodyne measurements are performed on the position/momentum quadratures of the ancilla qumodes, and the obtained measurement outcomes correspond to the syndrome values. Based on the obtained syndrome values, error localization and magnitude estimation are performed, followed by error correction implemented through displacement (D) gates.

Let us assume that the errors occurring on each qumode within the encoded block are given by

$$\boldsymbol{\epsilon} = \begin{bmatrix} \epsilon_{x1} & \epsilon_{p1} & \epsilon_{x2} & \epsilon_{p2} & \cdots & \epsilon_{x7} & \epsilon_{p7} \end{bmatrix}^\top, \tag{7}$$

where ϵ_x and ϵ_p denote displacement errors occur in the position and momentum quadratures of a single qumode, respectively.

According to the syndrome extraction circuit shown in Fig. 2, the expressions for the syndromes can be written as

$$\begin{aligned}
s_1 &= -\epsilon_{x1} + \epsilon_{x2} - \epsilon_{x5} - \epsilon_{x6} - 2\epsilon_{x7} + \hat{x}_2 + \hat{x}_{\text{anc1}}, \\
s_2 &= -\epsilon_{x1} + \epsilon_{x3} - \epsilon_{x5} - 2\epsilon_{x6} - \epsilon_{x7} + \hat{x}_3 + \hat{x}_{\text{anc2}}, \\
s_3 &= \epsilon_{x4} - \epsilon_{x5} - \epsilon_{x6} - \epsilon_{x7} + \hat{x}_4 + \hat{x}_{\text{anc3}}, \\
s_4 &= -\epsilon_{p2} - \epsilon_{p3} - \epsilon_{p4} - \epsilon_{p5} + \hat{x}_5 + \hat{p}_{\text{anc4}}, \\
s_5 &= \epsilon_{p1} - \epsilon_{p3} - \epsilon_{p4} - \epsilon_{p6} + \hat{x}_6 + \hat{p}_{\text{anc5}}, \\
s_6 &= \epsilon_{p1} - \epsilon_{p2} - \epsilon_{p4} - \epsilon_{p7} + \hat{x}_7 + \hat{p}_{\text{anc6}}.
\end{aligned} \tag{8}$$

Under ideal conditions, all qumodes except the one carrying the logical information are initialized in position/momentum eigenstates. Consequently, the mean and variance of $\hat{x}$ and $\hat{p}$ vanish, allowing all position/momentum operators in Eq. (8) to be neglected [34]. The syndrome expressions can therefore be simplified as

$$\begin{aligned}
s_1 &= -\epsilon_{x1} + \epsilon_{x2} - \epsilon_{x5} - \epsilon_{x6} - 2\epsilon_{x7}, \\
s_2 &= -\epsilon_{x1} + \epsilon_{x3} - \epsilon_{x5} - 2\epsilon_{x6} - \epsilon_{x7}, \\
s_3 &= \epsilon_{x4} - \epsilon_{x5} - \epsilon_{x6} - \epsilon_{x7}, \\
s_4 &= -\epsilon_{p2} - \epsilon_{p3} - \epsilon_{p4} - \epsilon_{p5}, \\
s_5 &= \epsilon_{p1} - \epsilon_{p3} - \epsilon_{p4} - \epsilon_{p6}, \\
s_6 &= \epsilon_{p1} - \epsilon_{p2} - \epsilon_{p4} - \epsilon_{p7}.
\end{aligned} \tag{9}$$

Assuming that the displacement errors of each qumode have a magnitude of unity, the corresponding syndrome values are summarized in Table I. Different error patterns yield distinct syndrome values, enabling unique identification of the error location and estimation of its magnitude. However, the lookup-based approach is inefficient in practice. To improve efficiency, a more direct analytical procedure for error localization and magnitude estimation is introduced.

Owing to the intrinsic property of Steane codes, the analyses of the position and momentum quadratures are decoupled. Hence, the following discussion focuses on the error localization and magnitude estimation in the position quadrature, while the momentum quadrature follows an analogous procedure and yields similar results, which are omitted for brevity. For the position quadrature, according to Eq. 9, the syndrome vector can be expressed as $\mathbf{s}_x = \mathbf{M}_x\boldsymbol{\epsilon}$. Here, $\mathbf{M}_x$ is

$$\mathbf{M}_x = \begin{bmatrix} -1 & 1 & 0 & 0 & -1 & -1 & -2 \\ -1 & 0 & 1 & 0 & -1 & -2 & -1 \\ 0 & 0 & 0 & 1 & -1 & -1 & -1 \end{bmatrix}. \tag{10}$$

Defining the column vector $\mathbf{m}_j$ as the jth column of $\mathbf{M}_x$, the following expression can be written as

$$T_j = \frac{\mathbf{m}_j^\top \mathbf{s}_x}{\|\mathbf{m}_j\|}. \tag{11}$$

According to the definition of T_j, the quantities T_1 through T_7 are evaluated individually, and the element with the largest absolute value is selected. The corresponding index j^* identifies the qumode on which the error occurs as

$$j^* = \arg\max_j |T_j|. \tag{12}$$

After the location of the error is identified, the magnitude of the displacement error $\hat{d}_{j^*}$ can be estimated as follows. By computing T_j and $\hat{d}_{j^*}$ in parallel, error localization and magnitude estimation can be efficiently performed.

$$\hat{d}_{j^*} = \frac{\mathbf{m}_{j^*}^\top \mathbf{s}_x}{\|\mathbf{m}_{j^*}\|^2}. \tag{13}$$

TABLE I. Syndrome values with the deterministic displacement magnitude ϵ taken as unity.

Error pattern	Position syndromes			Momentum syndromes		
	s_1	s_2	s_3	s_4	s_5	s_6
$\epsilon_{x1} = 1$	-1	-1	0	0	0	0
$\epsilon_{x2} = 1$	$+1$	0	0	0	0	0
$\epsilon_{x3} = 1$	0	$+1$	0	0	0	0
$\epsilon_{x4} = 1$	0	0	$+1$	0	0	0
$\epsilon_{x5} = 1$	-1	-1	-1	0	0	0
$\epsilon_{x6} = 1$	-1	-2	-1	0	0	0
$\epsilon_{x7} = 1$	-2	-1	-1	0	0	0
$\epsilon_{p1} = 1$	0	0	0	0	$+1$	$+1$
$\epsilon_{p2} = 1$	0	0	0	-1	0	-1
$\epsilon_{p3} = 1$	0	0	0	-1	-1	0
$\epsilon_{p4} = 1$	0	0	0	-1	-1	-1
$\epsilon_{p5} = 1$	0	0	0	-1	0	0
$\epsilon_{p6} = 1$	0	0	0	0	-1	0
$\epsilon_{p7} = 1$	0	0	0	0	0	-1

C. Logical Operation

To achieve universal quantum computation, it is necessary to implement fundamental quantum operations within the encoded Hilbert space [35, 36]. For CV systems, the basic quantum gates consist of the following

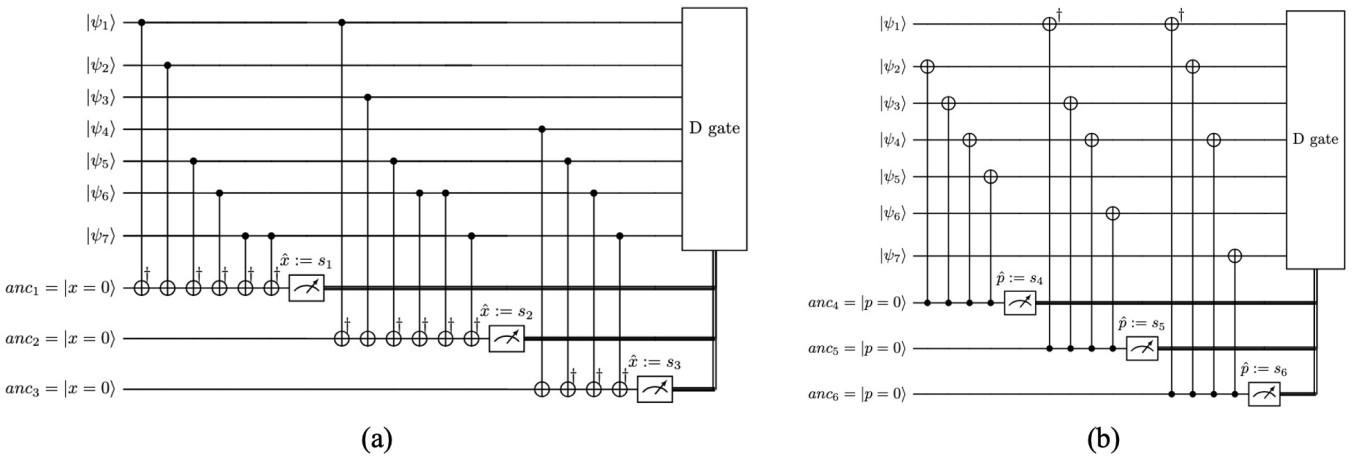

FIG. 2. (a) Position-quadrature syndrome extraction circuit. (b) Momentum-quadrature syndrome extraction circuit. Both circuits employ three ancilla qumodes, each initialized in a position or momentum eigenstate, respectively, to facilitate syndrome readout. Homodyne measurements are performed on the position/momentum quadratures of the ancilla qumodes, yielding syndromes $s_1 \sim s_6$. By analyzing these syndromes, the location and magnitude of the deterministic displacement errors can be identified, and the corresponding errors are corrected through displacement (D) gates.

Gaussian operations [11]: the displacement gate, the rotation gate, the single-mode squeezing gate, and the beam splitter. Other commonly used Gaussian operations, such as the two-mode squeezing gate and the SUM gate, can be constructed from combinations of beam splitters and single-mode squeezers, and are therefore not regarded as fundamental gates [37].

Gaussian operations preserve the Gaussian nature of states. However, universal quantum computation requires the inclusion of at least one non-Gaussian operation. A typical non-Gaussian operation is the cubic-phase gate [38]. In many practical architectures, the cubic-phase gate is not implemented as a native operation, but is instead typically realized via magic-state injection. In this approach, a specially prepared non-Gaussian resource state (the so-called magic state) is combined with Gaussian operations, measurement, and feed-forward to indirectly implement the cubic-phase transformation [39]. Consequently, the entire framework of universal quantum computation relies fundamentally on four Gaussian primitive gates.

Figure 3 shows the implementation circuits of the four fundamental logical Gaussian gates. In the DV Steane code, all logical Pauli operations are transversal and therefore inherently fault tolerant. In contrast, for the analog Steane code, the Hilbert space of each qumode lacks the periodic structure inherent to qubits, making it difficult to design transversal logical gates and thus to achieve fault-tolerant quantum computation. As illustrated in Fig. 3, only the logical displacement operation is fault tolerant, owing to its transversality, while other logical gates rely on entangling operations and are therefore non–fault tolerant (non-transversal). In the DV Steane code, all logical Clifford operations can be implemented transversally. This arises from the CSS structure defined

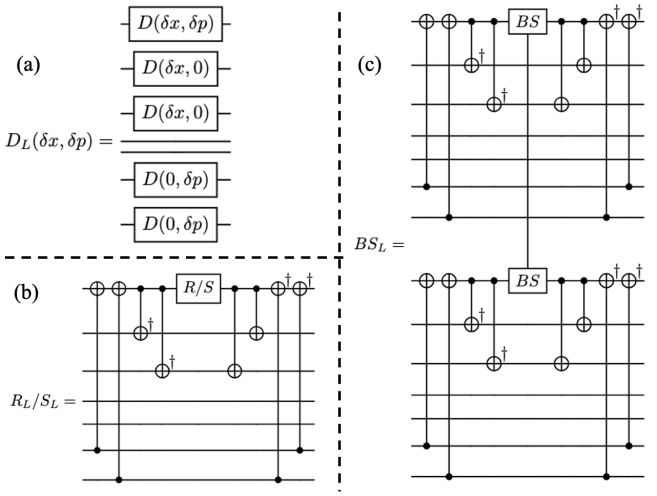

FIG. 3. Logical-operation circuits for (a) the displacement gate, (b) the rotation and squeezing gates, and (c) the beam splitter.

over the finite field $\mathbb{F}_2$, where the encoding matrix is orthogonal modulo 2. Local Clifford operations acting independently on each physical qubit induce the same logical transformations and preserve the stabilizer structure. In contrast, in the analog Steane code, logical Clifford operations correspond to Gaussian unitaries represented by real symplectic transformations in phase space. Except for the displacement gate, Gaussian operations such as rotation, squeezing, and beam splitter mix canonical variables across modes, leading to non-block-diagonal symplectic forms that destroy the tensor-product structure of the encoded subspace. Consequently, these operations cannot be applied independently to each mode and are

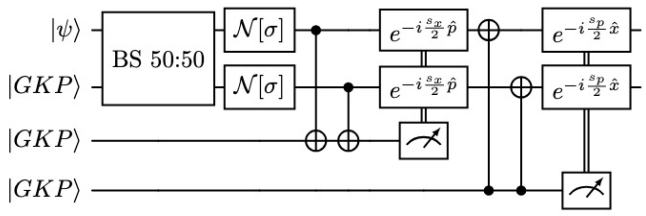

FIG. 4. Gaussian error suppression circuit.

nontransversal. Essentially, DV logical operations rely on discrete modular algebra that preserves mode independence, whereas CV logical operations are governed by continuous linear symplectic transformations that inherently involve mode coupling. As a result, transversal Clifford gates exist in the DV case, while only the displacement gate retains transversality in the CV case.

Designing fault-tolerant quantum error-correcting codes that can encode continuous logical information remains a significant challenge. A promising direction may involve hybrid CV–DV encodings that exploit the intrinsic periodicity of discrete-variable systems to overcome this limitation.

III. GAUSSIAN ERROR SUPPRESSION AND CONCATENATION TO EXPLOIT CODE DUALITY

To circumvent the constraint imposed by the no-go theorem [13], we introduce GKP states as non-Gaussian resources to suppress Gaussian displacement errors acting on all qumodes. For residual error beyond the suppression capability of the GKP layer, a concatenated analog Steane code is employed to further correct the remaining errors. In combination, these codes create a functional duality to correct arbitrary displacement errors, i.e., by providing additional functionality. In contrast, prior work on concatenation of quantum error correction codes aimed at lower logical error rates applying functionally equivalent techniques twice.

A. Gaussian Error Suppression Circuit

A 50:50 beam splitter is employed to entangle a data qumode with a GKP ancilla, as illustrated in Fig. 4. Gaussian displacement noise with a standard deviation of σ is injected into both the data and GKP qumodes, as indicated by the $\mathcal{N}[\sigma]$ symbols in the figure. For syndrome extraction, position and momentum eigenstates are respectively introduced to read out the syndrome outcomes on the position and momentum quadratures.

The Gaussian displacement errors acting on the two qumodes are denoted as

$$[\epsilon_{x,\text{data}},\, \epsilon_{p,\text{data}},\, \epsilon_{x,\text{GKP}},\, \epsilon_{p,\text{GKP}}]. \tag{14}$$

All displacement errors are assumed to follow independent Gaussian distributions, i.e.,

$$\epsilon \sim \mathcal{N}(0,\, \sigma^2), \tag{15}$$

where σ characterizes the standard deviation of the Gaussian noise in each quadrature. For an ideal GKP state, the spacing between adjacent wave packets is $2\sqrt{\pi}$. The corresponding expressions for the two syndromes in Fig. 4 are therefore given by

$$s_x = R_{2\sqrt{\pi}}(\epsilon_{x,\text{data}} + \epsilon_{x,\text{GKP}})\,, \tag{16}$$

$$s_p = R_{2\sqrt{\pi}}(-\epsilon_{p,\text{data}} - \epsilon_{p,\text{GKP}})\,, \tag{17}$$

where $R_{2\sqrt{\pi}}(\cdot)$ denotes the modulo operation that maps a real variable into the interval $[-\sqrt{\pi},\, \sqrt{\pi})$ with a period of $2\sqrt{\pi}$.

By subsequently applying controlled-displacement gates on the data and GKP qumodes, Gaussian errors can be effectively suppressed. In Sec. IV, we demonstrate that this suppression reduces the variance of the original Gaussian noise by a factor of two.

For the logical operations of this circuit, since the encoding operation consists only of a 50:50 beam splitter, all corresponding logical operations on the data mode can be expressed as

$$\hat{U}_L = \hat{B}^\dagger_{50:50}\, \hat{U}\, \hat{B}_{50:50}, \tag{18}$$

where $\hat{B}_{50:50}$ denotes the 50:50 beam splitter operation and $\hat{U}$ represents the corresponding physical-level operation.

B. Code Concatenation for Duality in Displacement

When the magnitude of a Gaussian displacement exceeds half of the GKP lattice spacing, the modulo operation maps the result into an incorrect interval, leading to a lattice-crossing error. Although such events occur with a relatively low probability, their impact is typically catastrophic, as they further amplify the magnitude of the underlying displacement error. Consequently, these errors lie beyond the correction capability of the circuit shown in Fig. 4. Our contribution here is to complement GPK via a concatenation construction with an outer analog Steane code, which can correct this type of large displacement error, thereby realizing duality in displacement functionality.

Specifically, the circuit is constructed by concatenating the analog Steane code shown in Fig. 1(b) with the Gaussian error-suppression circuit illustrated in Fig. 4. For each qumode within the encoding space of Fig. 1(b), a 50:50 beam splitter is used to entangle it with a GKP state, thereby forming the concatenated encoding circuit. This circuit naturally consists of two layers: the inner Gaussian error-suppression layer and the outer analog Steane layer. During the syndrome-extraction stage, the

inner layer first extracts syndromes to suppress Gaussian errors, while the outer analog Steane code detects and corrects other displacement errors.

For logical operations, since both the analog Steane code and the Gaussian error-suppression circuit have their respective logical operations well defined, the overall logical operation can be obtained by combining the two accordingly.

Previous concatenation schemes for bosonic codes, such as the GKP–repetition construction of Li and Su [9], convert biased Gaussian displacement noise into a discrete biased Pauli-$\bar{X}$ channel via a round of GKP error correction. They then apply a qubit-level repetition code with projective syndrome extraction that classifies measurement outcomes into Pauli-error zones and no-Pauli-error zones (i.e., by determining whether the residual displacement falls into phase-space regions associated with a logical Pauli flip or not) followed by digital majority voting. In contrast, our architecture operates at a fundamentally different level. We utilize the GKP layer solely as a Gaussian error-suppression mechanism that continuously reduces displacement variance on each mode, without collapsing errors into discrete Pauli events. Furthermore, the outer analog Steane code directly encodes continuous-variable logical information across multiple modes. Syndrome information in our scheme is obtained entirely through Gaussian circuits and homodyne detection. It is then processed as a full analog syndrome vector, enabling simultaneous inference of both the location and the magnitude of displacement errors, rather than only detecting whether a logical Pauli flip has occurred. This analog, CV-level decoding — combined with the dual-displacement structure of the code — allows our concatenated dual displacement code to jointly suppress small Gaussian fluctuations and rare lattice-crossing shifts within a single CV framework and using only one class of non-Gaussian resource (GKP ancillas), thereby going beyond DV-oriented GKP–repetition concatenations in both syndrome extraction strategy and operational scope.

IV. PERFORMANCE EVALUATION

This Section is organized as follows. Subsection IV A introduces the error model. Subsection IV B analyzes the performance of the concatenated code in the idealized setting, while Subsection IV C examines its performance under realistic conditions. Subsection IV D provides a detailed assessment of the experimental feasibility of implementing the concatenated code. Subsection IV E presents Monte–Carlo simulations that evaluate the code performance. Finally, Subsection IV F compares the proposed oscillator-based approach with schemes that encode an oscillator using qubits.

A. Error Model

Our concatenated scheme is inherently compatible with superconducting cavity-QED and trapped-ion platforms that feature long-lived bosonic modes, high-fidelity Gaussian operations, and access to non-Gaussian GKP resources. In the weak-noise regime, photon-loss, thermal-excitation, and dephasing channels can all be effectively modeled as Gaussian displacement noise in phase space, since their cumulative effect corresponds to random quadrature displacements characterized by Gaussian statistics [40]. Therefore, one of the primary noise sources considered in this work is Gaussian displacement error. Gaussian displacement error can be described as a statistical mixture of phase-space displacement operators whose amplitudes follow a Gaussian probability distribution [41]. The Gaussian displacement noise channel acts on any density matrix ρ as

$$\mathcal{E}_{\text{Gauss}}(\rho) = \int P(\delta)\, D(\delta)\, \rho\, D^{\dagger}(\delta)\, d\delta, \tag{19}$$

where $P(\delta)$ denotes a Gaussian distribution over displacements δ.

According to the no-go theorem, Gaussian displacement errors cannot be effectively suppressed using only Gaussian elements. Therefore, a Gaussian error-suppression circuit was designed in Sec. III. However, this circuit can suppress only those Gaussian errors whose magnitude does not exceed half of the GKP lattice spacing. Otherwise, a lattice-crossing error occurs.

In addition to Gaussian displacement noise, the proposed concatenated scheme can also correct occasional large-amplitude displacement errors, which we refer to as abrupt displacement errors. These rare but significant errors often stem from control pulse miscalibration, sudden flux or charge jumps, and other non-Gaussian noise events that intermittently disturb the oscillator dynamics [42, 43]. Unlike Gaussian noise, these events introduce abrupt, localized shifts in the quadrature amplitudes that can exceed the typical Gaussian error variance and lead to decoding failure if uncorrected.

B. Analysis under Ideal Conditions

The ideal condition refers to the case where all eigenstates and GKP states are assumed to be infinitely squeezed. The analysis under this assumption represents the theoretical limit that the code can achieve.

1. *Gaussian Error Suppression*

After the feedforward operation shown in Fig. 4, the residual displacement errors on the data and GKP qumodes are given by

$$\xi^{(\text{out})}_{x,\text{data}} = \epsilon_{x,\text{data}} - \tfrac{1}{2} R_{2\sqrt{\pi}}(\epsilon_{x,\text{data}} + \epsilon_{x,\text{GKP}})\,, \tag{20}$$

$$\xi^{(\mathrm{out})}_{p,\mathrm{data}} = \epsilon_{p,\mathrm{data}} - \tfrac{1}{2} R_{2\sqrt{\pi}}(\epsilon_{p,\mathrm{data}} + \epsilon_{p,\mathrm{GKP}})\,, \tag{21}$$

$$\xi^{(\mathrm{out})}_{x,\mathrm{GKP}} = \epsilon_{x,\mathrm{GKP}} - \tfrac{1}{2} R_{2\sqrt{\pi}}(\epsilon_{x,\mathrm{data}} + \epsilon_{x,\mathrm{GKP}})\,, \tag{22}$$

$$\xi^{(\mathrm{out})}_{p,\mathrm{GKP}} = \epsilon_{p,\mathrm{GKP}} - \tfrac{1}{2} R_{2\sqrt{\pi}}(\epsilon_{p,\mathrm{data}} + \epsilon_{p,\mathrm{GKP}})\,. \tag{23}$$

It can be seen that the expressions for each quadrature on the two qumodes are completely identical, forming a fully symmetric error-correction structure. Taking Eq. (20) as an example, the probability density function of the x quadrature on the data qumode is given by

$$X\left(\xi^{(\mathrm{out})}_{x,\mathrm{data}}\right) = \frac{1}{2\sqrt{\pi}\,\sigma} \sum_{m\in\mathbb{Z}} \exp\left[-\frac{\left(m\sqrt{\pi} - \xi^{(\mathrm{out})}_{x,\mathrm{data}}\right)^2}{\sigma^2}\right] \times \left[\mathrm{erf}\left(\frac{m\sqrt{\pi} + \frac{\sqrt{\pi}}{2}}{\sigma}\right) - \mathrm{erf}\left(\frac{m\sqrt{\pi} - \frac{\sqrt{\pi}}{2}}{\sigma}\right)\right]. \tag{24}$$

where $\mathrm{erf}(x) = \frac{2}{\sqrt{\pi}}\int_0^x e^{-t^2}\,dt$ is the error function.

Since $X\left(\xi^{(\mathrm{out})}_{x,\mathrm{data}}\right)$ is an even function, the mean value of the corresponding probability density function is $\mathbb{E}\left[\xi^{(\mathrm{out})}_{x,\mathrm{data}}\right] = \int \xi^{(\mathrm{out})}_{x,\mathrm{data}} X\left(\xi^{(\mathrm{out})}_{x,\mathrm{data}}\right) d\xi^{(\mathrm{out})}_{x,\mathrm{data}} = 0$.

The variance of the corresponding probability density function is given by

$$\mathrm{Var}\left(\xi^{(\mathrm{out})}_{x,\mathrm{data}}\right) = \frac{1}{2} \sum_{m\in\mathbb{Z}} \left(m^2\pi + \frac{\sigma^2}{2}\right) \times \left[\mathrm{erf}\left(\frac{m\sqrt{\pi} + \frac{\sqrt{\pi}}{2}}{\sigma}\right) - \mathrm{erf}\left(\frac{m\sqrt{\pi} - \frac{\sqrt{\pi}}{2}}{\sigma}\right)\right]. \tag{25}$$

A detailed derivation is provided in Appendix A, spanning Eqs. (A1)–(A5).

When the standard deviation of the Gaussian displacement noise is small ($\sigma \ll 1$), the $m = 0$ term dominates the summation, and contributions from $m \neq 0$ can be neglected. Therefore, the variance of the residual Gaussian noise can be expressed as

$$\sigma^2_{\mathrm{res}} = \sigma^2_{\mathrm{res},x} = \sigma^2_{\mathrm{res},p} = \mathrm{Var}\left(\xi^{(\mathrm{out})}_{x,\mathrm{data}}\right) \approx \tfrac{1}{2}\left(0 + \tfrac{\sigma^2}{2}\right) \times 2 = \tfrac{\sigma^2}{2}. \tag{26}$$

This result indicates that the Gaussian noise suppression circuit reduces the variance to half of its original value. However, it should be noted that the residual Gaussian noise can accumulate over successive QEC cycles, which may eventually lead to failure in long-duration quantum computation tasks due to the cumulative effect of noise.

2. *Concatenate Code*

The lattice structure of the GKP states enables the suppression of small displacement errors by correcting shifts within each unit cell. However, when the displacement magnitude exceeds half of the lattice spacing, a lattice-crossing event occurs. For the proposed concatenated code, the outer analog Steane code is responsible for correcting the lattice-crossing and abrupt errors. The composition of the analog Steane code's syndrome can be expressed as follows. Taking the position-quadrature syndrome as an example,

$$\mathbf{s}_x = \mathbf{M}_x\,\boldsymbol{\epsilon}_{\mathrm{res},x} + d\,\mathbf{m}_j. \tag{27}$$

Here, d denotes the magnitude of the lattice-crossing error, and $\boldsymbol{\epsilon}$ represents the residual Gaussian noise, which follows a normal distribution $\mathcal{N}(0, \sigma^2_{\mathrm{res}})$.

Equations (11) and (13) show the procedures for error localization and magnitude estimation without considering the residual Gaussian noise. When such residual noise is taken into account, the data should be whitened to improve the accuracy of both error localization and magnitude estimation [44]. Let the covariance matrix of the position-quadrature syndrome be denoted as $\boldsymbol{\Sigma}_{s_x}$, and define the whitening matrix as $\mathbf{W} = \boldsymbol{\Sigma}_{s_x}^{-1/2}$, yielding

$$T_j = \frac{\mathbf{m}_j^{\mathsf{T}} \boldsymbol{\Sigma}_{s_x}^{-1} \mathbf{s}_x}{\sqrt{\mathbf{m}_j^{\mathsf{T}} \boldsymbol{\Sigma}_{s_x}^{-1} \mathbf{m}_j}}, \tag{28}$$

$$\hat{d}_{j^*} = \frac{\mathbf{m}_{j^*}^{\mathsf{T}} \boldsymbol{\Sigma}_{s_x}^{-1} \mathbf{s}_x}{\mathbf{m}_{j^*}^{\mathsf{T}} \boldsymbol{\Sigma}_{s_x}^{-1} \mathbf{m}_{j^*}}. \tag{29}$$

For Eq. (13), the expectation and variance of its estimator are given by

$$\mathbb{E}\left[\hat{d}_{j^*}\right] = d, \qquad \mathrm{Var}\left(\hat{d}_{j^*}\right) = \frac{1}{\mathbf{m}_{j^*}^{\mathsf{T}} \boldsymbol{\Sigma}_{s_x}^{-1} \mathbf{m}_{j^*}}. \tag{30}$$

For qumodes within the analog Steane code block that do not experience lattice-crossing or abrupt errors, the position or momentum variance after one round of correction remains equal to the residual variance σ^2_{res} from the inner Gaussian-suppression circuit. For qumodes that experience a lattice-crossing error, the residual variance of their position or momentum quadrature is given by

$$\begin{aligned} \mathrm{Var}\left(\mathrm{qumode}_{j^*}\right) &= \sigma^2_{\mathrm{res}} + \mathrm{Var}\left(\hat{d}_{j^*}\right) - 2\,\mathrm{Cov}\left(\epsilon_{j^*}, \hat{d}_{j^*}\right) \\ &= \sigma^2_{\mathrm{res}} + \mathrm{Var}\left(\hat{d}_{j^*}\right) - 2\sigma^2_{\mathrm{res}} \\ &= \mathrm{Var}\left(\hat{d}_{j^*}\right) - \sigma^2_{\mathrm{res}}. \end{aligned} \tag{31}$$

For the position quadrature, when lattice-crossing or abrupt errors are sequentially considered on each qumode, the value of $\mathrm{Var}\left(\hat{d}_{j^*}\right) - 2\sigma^2_{\mathrm{res}}$ is summarized in Table II. It can be observed that when lattice-crossing or abrupt errors occur on qumodes 4, 6, and 7, the residual variances on these qumodes after error correction are lower than the residual Gaussian noise. This observation indicates that the analog Steane code is not a perfectly symmetric encoding structure.

TABLE II. Variance changes under lattice-crossing errors.

j^*	$\mathrm{Var}\left(\hat{d}_{j^*}\right) - 2\sigma_{\mathrm{res}}^2$
1	σ_{res}^2
2	σ_{res}^2
3	σ_{res}^2
4	$-\frac{2}{7}\sigma_{\mathrm{res}}^2$
5	$2\sigma_{\mathrm{res}}^2$
6	$-\frac{2}{7}\sigma_{\mathrm{res}}^2$
7	$-\frac{2}{7}\sigma_{\mathrm{res}}^2$

Another case must be considered: When the magnitude of a lattice-crossing or abrupt error becomes comparable to the residual Gaussian noise, the whitened error localization defined in Eq. (28) may lead to a miscorrection event. Miscorrection refers to the case where the error identified through the syndrome does not coincide with the actual physical error that occurred. Assume that the lattice-crossing or abrupt error actually occurs on qumode j but is misidentified as occurring on qumode k. Let the whitened position syndrome and corresponding pattern be $\tilde{\mathbf{s}}_x = \mathbf{W}\mathbf{s}_x$ and $\tilde{\boldsymbol{\mu}}_j = d\,\mathbf{W}\mathbf{m}_j$, respectively. If qumode j is correctly identified, then

$$\|\tilde{\mathbf{s}}_x - \tilde{\boldsymbol{\mu}}_j\|^2 \le \|\tilde{\mathbf{s}}_x - \tilde{\boldsymbol{\mu}}_k\|^2 \iff (\tilde{\boldsymbol{\mu}}_j - \tilde{\boldsymbol{\mu}}_k)^{\mathsf{T}}\left(\tilde{\mathbf{s}}_x - \tfrac{\tilde{\boldsymbol{\mu}}_j + \tilde{\boldsymbol{\mu}}_k}{2}\right) \ge 0. \tag{32}$$

Define $g_{jk} = (\tilde{\boldsymbol{\mu}}_j - \tilde{\boldsymbol{\mu}}_k)^{\mathsf{T}}\left(\tilde{\mathbf{s}}_x - \frac{\tilde{\boldsymbol{\mu}}_j + \tilde{\boldsymbol{\mu}}_k}{2}\right)$, which follows a Gaussian distribution:

$$\begin{aligned} &g_{jk} \sim \mathcal{N}\left(\tfrac{1}{2}\|\boldsymbol{\delta}_{jk}\|^2, \|\boldsymbol{\delta}_{jk}\|^2\right), \\ &\boldsymbol{\delta}_{jk} := \tilde{\boldsymbol{\mu}}_j - \tilde{\boldsymbol{\mu}}_k = d\,\mathbf{W}\left(\mathbf{m}_j - \mathbf{m}_k\right). \end{aligned} \tag{33}$$

When qumode j is misidentitied as qumode k, the probability of this event is given by

$$\Pr(j \to k) = \Pr(g_{jk} < 0) = Q\left(\tfrac{1}{2}\|\boldsymbol{\delta}_{jk}\|\right), \tag{34}$$

where $Q(x) = \frac{1}{\sqrt{2\pi}}\int_x^\infty e^{-t^2/2}\,dt$ is the right tail of the standard normal distribution. Expanding the expression of $\boldsymbol{\delta}_{jk}$ yields

$$\|\boldsymbol{\delta}_{jk}\|^2 = d^2(\mathbf{m}_j - \mathbf{m}_k)^{\mathsf{T}}\boldsymbol{\Sigma}_{s_x}^{-1}(\mathbf{m}_j - \mathbf{m}_k) = d^2\,\Delta_{jk}^2. \tag{35}$$

$$\Pr(j \to k) = Q\left(\frac{d}{2}\sqrt{\Delta_{jk}^2}\right). \tag{36}$$

According to Eq. (36), the probability of a miscorrection event where qumode j is identified as all $k \neq j$ satisfies

$$P_{\mathrm{miscorr}}^{(j)} \le \sum_{k \neq j} Q\left(\frac{d}{2}\sqrt{\Delta_{jk}^2}\right). \tag{37}$$

As shown in Fig. 5, the miscorrection probability $P_{\mathrm{miscorr}}^{(j)}$ in both the position and momentum quadratures depends on the ratio between the displacement error magnitude d and the residual Gaussian noise standard deviation σ_{res}. As d/σ_{res} increases, $P_{\mathrm{miscorr}}^{(j)}$ decreases rapidly. When $d/\sigma_{\mathrm{res}} \approx 10$, the value of $P_{\mathrm{miscorr}}^{(j)}$ approaches zero, indicating that miscorrection events are essentially eliminated.

C. Analysis under Real Conditions

In realistic conditions, both eigenstates and GKP states are finitely squeezed, which introduces additional uncertainty into the proposed concatenated code. For the inner Gaussian-error-suppression circuit, a finitely squeezed GKP state can be regarded as an ideal GKP state superimposed with an additional Gaussian noise whose variance depends on the squeezing strength. Similarly, the position or momentum eigenstates become finitely squeezed vacuum states.

Let the squeezing parameter be denoted by r. The variance along the squeezed quadrature can then be expressed as $\frac{1}{2}e^{-2r}$, which also corresponds to the variance of each peak in a finitely squeezed GKP state. Similar to Eqs. (24)–(26), under finite squeezing, the residual Gaussian noise variance on the data qumodes of the Gaussian-error-suppression circuit is given by

$$\sigma_{\mathrm{res}}^2 = \tfrac{1}{2}\sigma^2 + \tfrac{1}{8}e^{-2r} + \mathcal{O}\left(R_{2\sqrt{\pi}}(\cdot)\right), \tag{38}$$

where the term $\mathcal{O}\left(R_{2\sqrt{\pi}}(\cdot)\right)$ represents the additional error contribution caused by lattice crossing, which becomes negligible when σ is small. Therefore, from Eq. (38), it can be seen that an error-suppression gain can be achieved when $r > -\ln(2\sigma)$.

For the outer analog Steane code, taking the position quadrature as an example, the expression for the syndrome is modified from Eq. (27) to

$$\mathbf{s}_x = \mathbf{M}_x\boldsymbol{\epsilon}_{\mathrm{res},x} + d\,\mathbf{m}_j + \mathbf{A}_x\mathbf{n}_x. \tag{39}$$

where $\mathbf{n}_x = [\hat{x}_2, \hat{x}_3, \hat{x}_4, \hat{x}_{\mathrm{anc1}}, \hat{x}_{\mathrm{anc2}}, \hat{x}_{\mathrm{anc3}}]^{\mathsf{T}}$, each position operator has a variance of $\frac{1}{2}e^{-2r}$, and $\mathbf{A}_x$ is given by

$$\mathbf{A}_x = \begin{bmatrix} 1 & 0 & 0 & 1 & 0 & 0 \\ 0 & 1 & 0 & 0 & 1 & 0 \\ 0 & 0 & 1 & 0 & 0 & 1 \end{bmatrix}. \tag{40}$$

In the error localization (Eq. (28)) and magnitude estimation (Eq. (29)), the covariance matrix of $\mathbf{s}_x$ is utilized. According to Eq. (39), the updated covariance matrix is given by

$$\boldsymbol{\Sigma}_{s_x} = \sigma_{\mathrm{res}}^2\mathbf{M}_x\mathbf{M}_x^{\mathsf{T}} + \tfrac{1}{2}e^{-2r}\mathbf{A}_x\mathbf{A}_x^{\mathsf{T}}. \tag{41}$$

Through the covariance matrix $\boldsymbol{\Sigma}_{s_x}$, one can qualitatively analyze how the key parameters vary with the squeezing parameter r. Equation (29) gives the variance of the estimated magnitude of the lattice-crossing error,

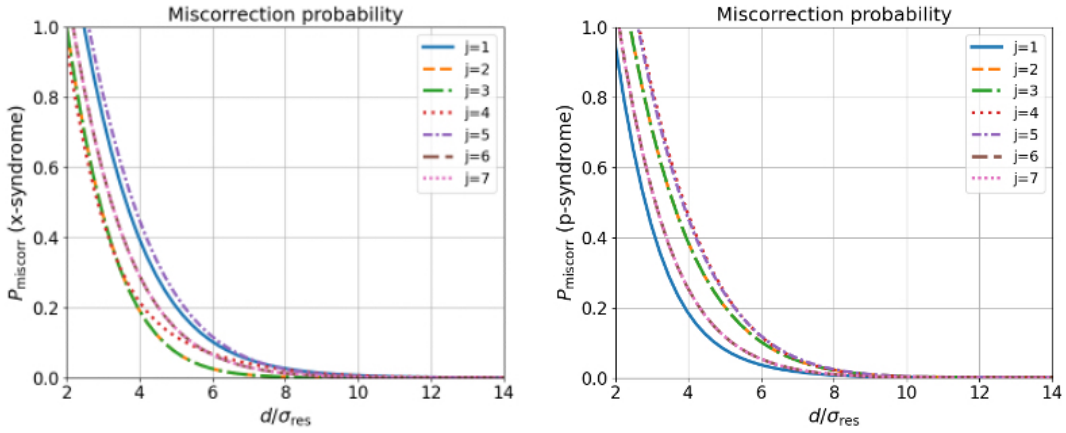

FIG. 5. The miscorrection probability $P^{(j)}_{\text{miscorr}}$. The left panel corresponds to the position quadrature, and the right panel corresponds to the momentum quadrature. Each curve corresponds to a representative qumode, where the miscorrection probability rapidly decreases as d/σ_{res} increases.

whose derivative is

$$\frac{d}{dr}\text{Var}(\hat{d}_{j^*}) = -\frac{1}{\left(\mathbf{m}_{j^*}^T \mathbf{\Sigma}_{s_x}^{-1} \mathbf{m}_{j^*}\right)^2} \frac{d}{dr}\left(\mathbf{m}_{j^*}^T \mathbf{\Sigma}_{s_x}^{-1} \mathbf{m}_j\right)$$
$$= -\frac{1}{\left(\mathbf{m}_{j^*}^T \mathbf{\Sigma}_{s_x}^{-1} \mathbf{m}_{j^*}\right)^2} \left(2e^{-2r}\, \mathbf{m}_j^T \mathbf{\Sigma}_{s_x}^{-2} \mathbf{m}_j\right) < 0. \tag{42}$$

As the squeezing strength increases, the variance of the estimated error magnitude decreases, indicating that stronger squeezing enhances the performance of the analog Steane code. Similarly, one can infer that the probability of miscorrection also decreases with increasing squeezing strength, thereby reducing the risk of catastrophic failures caused by error miscorrection.

D. Experimental Feasibility

The concatenated encoding architecture with its functional duality under consideration employs an analog Steane code as the outer layer to correct lattice-crossing and abrupt errors, and GKP states as the inner layer to suppress Gaussian displacement error. Crucially, apart from the preparation of approximate GKP states, no other non-Gaussian resources are required.

Squeezed optical modes with moderate levels of squeezing (e.g., $r \sim 10$–12 dB) are already routinely achieved in modern CV platforms [45]. In our scheme, the outer analog Steane code can be implemented entirely with Gaussian operations (beam splitters, SUM gate, Fourier gate, homodyne detection and feed-forward) plus the injection of GKP ancilla modes. Since the only non-Gaussian element is the finite-energy GKP state, the experimental overhead is significantly reduced compared to schemes relying on large numbers of non-Gaussian gates.

Recent theoretical works on concatenated GKP-based codes have established that error suppression becomes feasible once the GKP squeezing surpasses a threshold on the order of 10–15 dB under realistic noise assumptions [19, 46]. Given that our concatenation further leverages the analog Steane code to absorb residual displacement errors, the required GKP resource quality is relaxed, making the scheme experimentally accessible in the near term.

TABLE III. Effective Gaussian noise levels and lattice-crossing probabilities for representative physical platforms.

Platform	Effective Gaussian noise variance	Lattice-crossing probability
Optical CV [50]	~ 0.005	0.016%
cQED [49]	~ 0.02	0.081%
Trapped-ion [48]	~ 0.03	0.17%
Optomechanics [47]	~ 0.2	7.6%

We summarize in Table III the levels of Gaussian displacement noise variance per single QEC round across different experimental platforms [47–50]. For some platforms, the reported values are obtained through subsequent conversions. For instance, the result for the trapped-ion platform is inferred from the measured motional heating rate. Table III presents the corresponding noise variances and lattice-crossing probabilities for a GKP state with a squeezing level of 10 dB across various platforms. The probability of a lattice-crossing error is evaluated using $\text{erfc}\left(\frac{\sqrt{\pi}}{2\sqrt{2\sigma}}\right)$, which represents the two-tailed Gaussian probability that the displacement magnitude exceeds $\sqrt{\pi}/2$. Among these platforms, the optomechanical system is significantly affected by Gaussian noise, which constitutes one of its dominant noise sources. In contrast, other platforms exhibit lattice-crossing probabilities well below 1%. However, as the number of qumodes increases, this probability grows exponentially, and thus remains non-negligible.

In a cQED platform, the proposed concatenated code is estimated to take about 7 μs for a single round, assuming highly parallelized gate scheduling. This estimate is based on characteristic operation times of 150 ns for a SUM gate [51], 20 ns for a displacement gate [52], and 1100 ns for a homodyne measurement [53]. Given the superconducting resonator lifetimes of 250–350 μs achieved on the Yale cQED platform [49], multiple QEC rounds can be executed well within the coherence window, thereby further enhancing the logical lifetime of the protected information.

Key experimental considerations include: Preparation of approximate GKP states with fidelity sufficient to reduce inner-layer miscorrection probabilities below the outer-layer decoding threshold is achieved. Optical losses and finite detection efficiencies must be kept low enough such that the effective displacement noise entering the outer Steane layer remains within the correctable regime. Feed-forward latency and stability of Gaussian elements rely on the architecture implementing real-time displacement corrections based on syndrome measurements, which is well within the performance of current CV optics platforms.

In summary, the proposed concatenated architecture requires only one class of non-Gaussian resource (the GKP state) while all other operations remain Gaussian. With moderate squeezing levels and high-efficiency Gaussian measurement/detection, the full setup is within reach of current or near-term continuous-variable quantum optics experiments.

E. Simulation Results

To illustrate the error-suppression capabilities of different circuit levels under idealized conditions (i.e., infinite squeezing), we performed Monte Carlo simulations for three scenarios: (i) no QEC applied to the data qumode, (ii) Gaussian-noise suppression using the circuit in Fig. 4, and (iii) the full concatenated code. These simulations provide an intuitive comparison of how each mechanism mitigates displacement noise.

In the baseline case without any QEC, the data qumode receives, in every QEC round, a displacement error (restricted to the position quadrature in our simulation) drawn from a Gaussian distribution with variance 0.2. When the Gaussian-noise–suppression circuit of Fig. 4 is applied, both the data qumode and the ancilla GKP states are subjected to displacement errors independently sampled from the same variance given by 0.2 of a Gaussian distribution. For the concatenated-code scenario, every data qumode and every GKP ancilla qumode experiences an independently sampled displacement error drawn from a Gaussian distribution of variance 0.2.

In addition to Gaussian noise, all three scenarios include an abrupt displacement error of fixed magnitude $+2\sqrt{\pi}$, which induces a lattice-crossing event. Because the analog Steane code has a limited ability to correct such abrupt shifts, this error is applied only to the first data qumode, and our simulation results focus on the residual-displacement distribution of that mode.

As a figure of merit, we use the residual displacement on the data qumode, denoted by ζ_{res}, to quantify the remaining noise after each QEC round. For every scenario, a total of $2,000$ Monte Carlo samples are generated to obtain the empirical distribution of ζ_{res}. Figure 6 shows the residual displacement distributions for the three scenarios. The blue solid curve represents the mean residual displacement in the current QEC round, $\zeta_{\text{res,mean}}$, obtained by averaging over all Monte Carlo samples. The black dashed curve represents the combination of the sample standard deviation σ_{current} and the mean value $\zeta_{\text{res,mean}}$ for that round. The quantity $\zeta_{\text{res,mean}} \pm \sigma_{\text{current}}$ characterizes both the cumulative drift and the spread of the residual noise as the number of QEC rounds increases.

In Fig. 6, an abrupt displacement error is injected every 100 QEC rounds. In Fig. 6(a), where no QEC is applied, one observes a pronounced accumulation of error: the variance of the residual displacement grows steadily with the number of rounds, and beyond a certain point the data qumode becomes excessively noisy and effectively unusable. In Fig. 6(b), because Gaussian-error suppression alone cannot correct abrupt displacements, each injection produces a lattice-crossing event, leading to the periodic jumps in the mean residual displacement visible in both Figs. 6(a) and 6(b).

A comparison between panels (a) and (b) shows that the scenario with Gaussian error suppression exhibits significantly reduced diffusion of the residual displacement relative to the no-QEC case. After 1,000 rounds, the sample standard deviations of the residual displacement are 14.14 and 10.19 for the two scenarios, respectively, yielding a variance-suppression ratio of 0.52, in good agreement with the theoretical prediction of Eq. (26).

A comparison between Figures 6(b) and 6(c) shows that adding the outer analog Steane code enables effective correction of the injected abrupt displacement errors. In Fig. 6(c), the mean residual displacement remains centered around zero despite the periodic injections, demonstrating the code's ability to suppress such large shifts. The final standard deviation of the residual displacement in panel (c) is 10.20, essentially identical to the value observed in panel (b), indicating that the Gaussian-noise–suppression performance is preserved while abrupt errors are corrected.

In the context of bosonic quantum error correction, it is common to inquire if a coding scheme admits a fault-tolerance threshold, i.e., a physical noise level below which repeated QEC can, in principle, drive the logical displacement noise arbitrarily close to zero. However, as established rigorously in [54], no oscillator-to-oscillator code operating under finite squeezing can exhibit such a threshold. Because the concatenated construction studied here is subject to the same squeezing constraints, it likewise does not possess a fundamental threshold, even though displacement noise may be reduced within a lim-

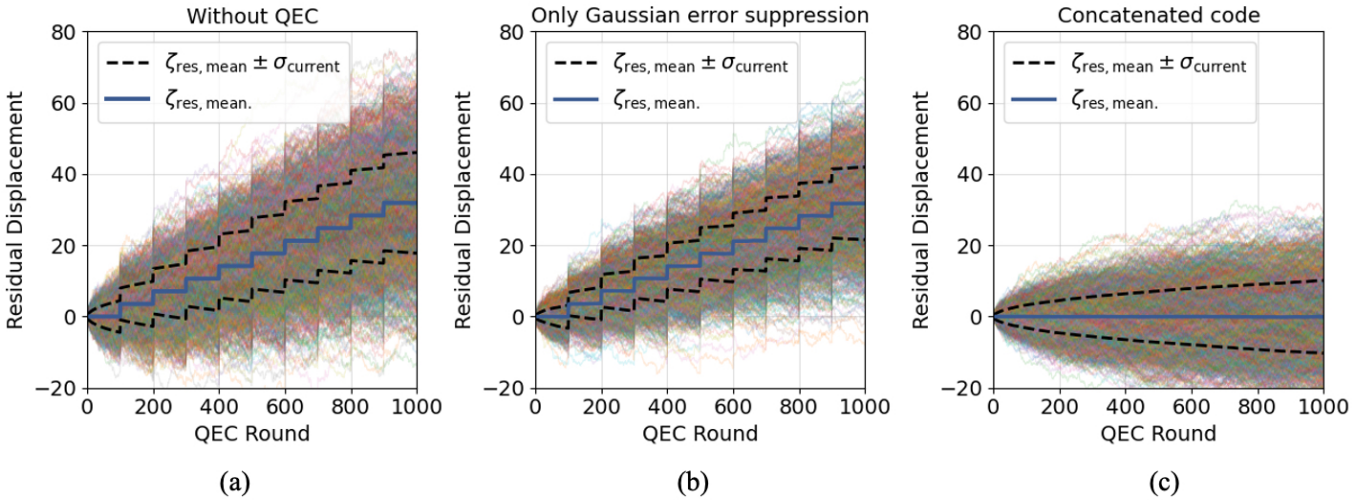

FIG. 6. Monte Carlo simulation of the residual displacement ζ_{res} on the data qumode over $1,000$ QEC rounds for the three scenarios considered: (a) no QEC, (b) Gaussian-noise suppression only, and (c) the full concatenated code. An biased abrupt displacement of magnitude $+2\sqrt{\pi}$ is intentionally applied every 100 QEC rounds. Each panel shows $2,000$ individual trajectories (faint curves), the mean value $\zeta_{\text{res,mean}}$ (blue solid line), and the interval $\zeta_{\text{res,mean}} \pm \sigma_{\text{current}}$ (black dashed lines), where σ_{current} is the sample standard deviation in the corresponding round.

ited operational regime.

F. Comparison with qubit-based oscillator encoding

An alternative approach to representing a bosonic oscillator is to digitally encode its Hilbert space into multiple two-level systems. In such qubit-based simulations, the oscillator's infinite-dimensional Fock basis is truncated to a finite dimension N, and each truncated level $|n\rangle$ is represented by a binary string over $\log_2 N$ qubits. This DV representation enables the emulation of CV dynamics on qubit-based platforms, and has been explored in the context of digital quantum simulation and bosonic mode encoding [55].

However, such qubit-based encodings require a large number of physical qubits to faithfully capture the dynamics of even a single bosonic mode, especially when representing high photon-number states or fine phase-space structures such as those in GKP lattices. Moreover, the mapping from CV operators (e.g., $\hat{x}, \hat{p}$) to qubit operators is nonlocal and introduces additional circuit overhead for basic Gaussian transformations, such as displacements, beam splitters, and squeezers. These factors significantly increase both the hardware and gate-time resources required to simulate oscillator-level QEC processes.

In contrast, the present CV-based encoding directly employs a single physical oscillator as the logical carrier, leveraging its native continuous Hilbert space. This approach naturally supports Gaussian operations and homodyne-based measurements, thus avoiding the need for qubit-level digital approximations. Furthermore, when concatenated with a GKP layer, the proposed CV code inherits both the fine-grained phase-space protection of the GKP lattice and the scalable syndrome structure of higher-level bosonic codes, achieving error suppression with substantially fewer physical resources compared to qubit-based oscillator encodings.

Overall, while qubit-based digital encodings offer a universal route to simulating oscillators, the direct CV approach pursued here provides a more hardware-efficient and physically transparent path toward implementing continuous-variable quantum error correction in realistic cQED and optomechanical architectures.

V. CONCLUSION

In this work, we have presented a concatenated CV quantum error-correcting framework where a analog Steane code is combined with GKP-based Gaussian error suppression. The construction realizes duality in the codes in that the inner GKP layer mitigates Gaussian displacement noise, while the outer analog Steane code corrects lattice-crossing and abrupt errors that occur beyond the suppression capability of the GKP layer. Most of our analytical derivations have been conducted under idealized conditions with infinitely squeezed states, establishing the theoretical upper limit of the proposed architecture.

By analyzing the residual noise variance and the covariance structure under finite squeezing, we demonstrated that the concatenated design enables simultaneous suppression of Gaussian and abrupt displacement errors, thus overcoming the Gaussian no-go constraint. The results further show that the residual variance decreases

monotonically with the squeezing strength, indicating enhanced precision in error localization and magnitude estimation. Although a quantitative threshold for the GKP squeezing was not specified, the outer analog Steane code effectively relaxes the resource requirement for the inner GKP layer, suggesting reduced experimental overhead.

Experimentally, the architecture requires only one non-Gaussian resource, the GKP state, while all other operations remain Gaussian and compatible with existing optical and superconducting CV platforms. This feature highlights the feasibility of near-term experimental demonstrations once approximate GKP states with sufficient fidelity become available.

Future research will focus on exploring alternative non-Gaussian resources for Gaussian-noise suppression and on developing hybrid CV–DV concatenation schemes to further enhance robustness against realistic noise in scalable quantum information processors.

ACKNOWLEDGMENTS

This work is supported by the U.S. Department of Energy, Office of Science, Advanced Scientific Computing Research, under contract number DE-SC0025384. This work was also funded in part by NSF grants OMA-2120757, NSF PHY-2325080, OSI-2410675.

Appendix A: Derivation of the Gaussian Error Suppression Formula

The probability density function of Eq. (20) can be expressed as

$$
\begin{aligned}
X\left(\xi^{(\mathrm{out})}_{x,\mathrm{data}}\right) &= \frac{1}{2\pi\sigma^2}\iint \delta\Big(\xi^{(\mathrm{out})}_{x,\mathrm{data}} - \epsilon_{x,\mathrm{data}} + \tfrac{1}{2}R_{2\sqrt{\pi}}(\epsilon_{x,\mathrm{data}}+\epsilon_{x,\mathrm{GKP}})\Big) \\
&\qquad \times \exp\left[-\frac{\epsilon^2_{x,\mathrm{data}}+\epsilon^2_{x,\mathrm{GKP}}}{2\sigma^2}\right] d\epsilon_{x,\mathrm{data}}\, d\epsilon_{x,\mathrm{GKP}} \\
&= \sum_{m\in\mathbb{Z}} \iint_{\epsilon_{x,\mathrm{data}}+\epsilon_{x,\mathrm{GKP}}\in[\,2m\sqrt{\pi}-\sqrt{\pi},\,2m\sqrt{\pi}+\sqrt{\pi}\,)} \frac{1}{2\pi\sigma^2}\,\delta\Big(\xi^{(\mathrm{out})}_{x,\mathrm{data}} - \tfrac{1}{2}\epsilon_{x,\mathrm{data}} + \tfrac{1}{2}\epsilon_{x,\mathrm{GKP}} - m\sqrt{\pi}\Big) \\
&\qquad \times \exp\left[-\frac{\epsilon^2_{x,\mathrm{data}}+\epsilon^2_{x,\mathrm{GKP}}}{2\sigma^2}\right] d\epsilon_{x,\mathrm{data}}\, d\epsilon_{x,\mathrm{GKP}} \\
&= \frac{1}{\pi\sigma^2}\sum_{m\in\mathbb{Z}} \int_{2m\sqrt{\pi}-\frac{\sqrt{\pi}}{2}-\xi^{(\mathrm{out})}_{x,\mathrm{data}}}^{2m\sqrt{\pi}+\frac{\sqrt{\pi}}{2}-\xi^{(\mathrm{out})}_{x,\mathrm{data}}} \\
&\qquad \exp\left[-\frac{\left(2\xi^{(\mathrm{out})}_{x,\mathrm{data}}+\epsilon_{x,\mathrm{GKP}}-2m\sqrt{\pi}\right)^2+\epsilon^2_{x,\mathrm{GKP}}}{2\sigma^2}\right] d\epsilon_{x,\mathrm{GKP}} \\
&= \frac{1}{\pi\sigma^2}\sum_{m\in\mathbb{Z}} \exp\left[-\frac{\left(m\sqrt{\pi}-\xi^{(\mathrm{out})}_{x,\mathrm{data}}\right)^2}{\sigma^2}\right] \int_{2m\sqrt{\pi}-\frac{\sqrt{\pi}}{2}-\xi^{(\mathrm{out})}_{x,\mathrm{data}}}^{2m\sqrt{\pi}+\frac{\sqrt{\pi}}{2}-\xi^{(\mathrm{out})}_{x,\mathrm{data}}} \\
&\qquad \exp\left[-\frac{\left(\epsilon_{x,\mathrm{GKP}}-(m\sqrt{\pi}-\xi^{(\mathrm{out})}_{x,\mathrm{data}})\right)^2}{\sigma^2}\right] d\epsilon_{x,\mathrm{GKP}} \\
&= \frac{1}{2\sqrt{\pi}\,\sigma}\sum_{m\in\mathbb{Z}} \exp\left[-\frac{\left(m\sqrt{\pi}-\xi^{(\mathrm{out})}_{x,\mathrm{data}}\right)^2}{\sigma^2}\right]\left[\mathrm{erf}\left(\frac{m\sqrt{\pi}+\frac{\sqrt{\pi}}{2}}{\sigma}\right)-\mathrm{erf}\left(\frac{m\sqrt{\pi}-\frac{\sqrt{\pi}}{2}}{\sigma}\right)\right],
\end{aligned}
\tag{A1}
$$

where $\mathrm{erf}(x)=\frac{2}{\sqrt{\pi}}\int_0^x e^{-t^2}\,dt$ is the error function.

The variance of the corresponding probability density function is given by

$$
\begin{aligned}
\mathrm{Var}\left(\xi^{(\mathrm{out})}_{x,\mathrm{data}}\right) &= \int \left(\xi^{(\mathrm{out})}_{x,\mathrm{data}}\right)^2 X\left(\xi^{(\mathrm{out})}_{x,\mathrm{data}}\right)\, d\xi^{(\mathrm{out})}_{x,\mathrm{data}} \\
&= \frac{1}{2\sqrt{\pi}\,\sigma}\sum_{m\in\mathbb{Z}}\left[\mathrm{erf}\left(\frac{m\sqrt{\pi}+\frac{\sqrt{\pi}}{2}}{\sigma}\right)-\mathrm{erf}\left(\frac{m\sqrt{\pi}-\frac{\sqrt{\pi}}{2}}{\sigma}\right)\right] \\
&\qquad \times \int_{-\infty}^{\infty}\left(\xi^{(\mathrm{out})}_{x,\mathrm{data}}\right)^2 \exp\left[-\frac{\left(\xi^{(\mathrm{out})}_{x,\mathrm{data}}-m\sqrt{\pi}\right)^2}{\sigma^2}\right] d\xi^{(\mathrm{out})}_{x,\mathrm{data}}.
\end{aligned}
\tag{A2}
$$

To further simplify the expression for $\mathrm{Var}\left(\xi^{(\mathrm{out})}_{x,\mathrm{data}}\right)$, we define

$$J_m = \int_{-\infty}^{\infty} \left(\xi^{(\mathrm{out})}_{x,\mathrm{data}}\right)^2 \exp\left[-\frac{\left(\xi^{(\mathrm{out})}_{x,\mathrm{data}} - m\sqrt{\pi}\right)^2}{\sigma^2}\right] d\xi^{(\mathrm{out})}_{x,\mathrm{data}}. \tag{A3}$$

Then,

$$\begin{aligned} J_m = &\int_{-\infty}^{\infty} \left(\xi^{(\mathrm{out})}_{x,\mathrm{data}} - m\sqrt{\pi}\right)^2 \exp\left[-\frac{\left(\xi^{(\mathrm{out})}_{x,\mathrm{data}} - m\sqrt{\pi}\right)^2}{\sigma^2}\right] d\xi^{(\mathrm{out})}_{x,\mathrm{data}} \\ &+ 2m\sqrt{\pi}\int_{-\infty}^{\infty} \left(\xi^{(\mathrm{out})}_{x,\mathrm{data}} - m\sqrt{\pi}\right) \exp\left[-\frac{\left(\xi^{(\mathrm{out})}_{x,\mathrm{data}} - m\sqrt{\pi}\right)^2}{\sigma^2}\right] d\xi^{(\mathrm{out})}_{x,\mathrm{data}} \\ &+ m^2\pi \int_{-\infty}^{\infty} \exp\left[-\frac{\left(\xi^{(\mathrm{out})}_{x,\mathrm{data}} - m\sqrt{\pi}\right)^2}{\sigma^2}\right] d\xi^{(\mathrm{out})}_{x,\mathrm{data}} \\ = &\sqrt{\pi}\,\sigma\left(m^2\pi + \frac{\sigma^2}{2}\right). \end{aligned} \tag{A4}$$

Therefore, we obtain

$$\begin{aligned} \mathrm{Var}\left(\xi^{(\mathrm{out})}_{x,\mathrm{data}}\right) = &\frac{1}{2}\sum_{m\in\mathbb{Z}}\left(m^2\pi + \frac{\sigma^2}{2}\right) \\ &\times\left[\mathrm{erf}\left(\frac{m\sqrt{\pi} + \frac{\sqrt{\pi}}{2}}{\sigma}\right) - \mathrm{erf}\left(\frac{m\sqrt{\pi} - \frac{\sqrt{\pi}}{2}}{\sigma}\right)\right]. \end{aligned} \tag{A5}$$

[1] P. W. Shor, Scheme for reducing decoherence in quantum computer memory, Phys. Rev. A **52**, R2493 (1995).
[2] A. M. Steane, Error correcting codes in quantum theory, Phys. Rev. Lett. **77**, 793 (1996).
[3] D. Gottesman, *Stabilizer Codes and Quantum Error Correction*, Ph.D. thesis, California Institute of Technology (1997), arXiv:quant-ph/9705052.
[4] W. Cai, Y. Ma, W. Wang, C.-L. Zou, and L. Sun, Bosonic quantum error correction codes in superconducting quantum circuits, Fundam. Res. **1**, 50 (2021).
[5] A. G. Fowler, M. Mariantoni, J. M. Martinis, and A. N. Cleland, Surface codes: Towards practical large-scale quantum computation, Phys. Rev. A **86**, 032324 (2012).
[6] G. Q. AI, Suppressing quantum errors by scaling a surface code logical qubit, Nature **614**, 676 (2023).
[7] Y. Xu, Y. Wang, E.-J. Kuo, and V. V. Albert, Qubit-oscillator concatenated codes: Decoding formalism and code comparison, PRX Quantum **4**, 020342 (2023).
[8] M. P. Stafford and N. C. Menicucci, Biased gottesman-kitaev-preskill repetition code, Phys. Rev. A **108**, 052428 (2023).
[9] Z. Li and D. Su, Correcting biased noise using gottesman-kitaev-preskill repetition code with noisy ancilla, Phys. Rev. A **109**, 052420 (2024).
[10] S. L. Braunstein and P. van Loock, Quantum information with continuous variables, Rev. Mod. Phys. **77**, 513 (2005).
[11] C. Weedbrook, S. Pirandola, R. García-Patrón, N. J. Cerf, T. C. Ralph, J. H. Shapiro, and S. Lloyd, Gaussian quantum information, Rev. Mod. Phys. **84**, 621 (2012).
[12] A. Blais, A. L. Grimsmo, S. M. Girvin, and A. Wallraff, Circuit quantum electrodynamics, Rev. Mod. Phys. **93**, 025005 (2021).
[13] J. Niset, J. Fiurášek, and N. J. Cerf, No-go theorem for gaussian quantum error correction, Phys. Rev. Lett. **102**, 120501 (2009).
[14] B. M. Terhal, Quantum error correction for quantum memories, Rev. Mod. Phys. **87**, 307 (2015).
[15] Y. Xu, Y. Wang, E.-J. Kuo, and V. V. Albert, Qubit-oscillator concatenated codes: Decoding formalism and code comparison, PRX Quantum **4**, 020342 (2023).
[16] D. Gottesman, A. Kitaev, and J. Preskill, Encoding a qubit in an oscillator, Phys. Rev. A **64**, 012310 (2001).
[17] S. Glancy and E. Knill, Error analysis for encoding a qubit in an oscillator, Phys. Rev. A **73**, 012325 (2006).
[18] K. Fukui, A. Tomita, A. Okamoto, and K. Fujii, High-threshold fault-tolerant quantum computation with analog quantum error correction, Phys. Rev. X **8**, 021054 (2018).
[19] K. Noh, S. M. Girvin, and L. Jiang, Encoding an oscillator into many oscillators, Phys. Rev. Lett. **125**, 080503 (2020).

[20] S. L. Braunstein, Error correction for continuous quantum variables, Phys. Rev. Lett. **80**, 4084 (1998).

[21] T. Aoki, G. Takahashi, T. Kajiya, J. Yoshikawa, S. L. Braunstein, P. van Loock, and A. Furusawa, Quantum error correction beyond qubits, Nat. Phys. **5**, 541 (2009).

[22] A. Schuckert, E. Crane, A. V. Gorshkov, M. Hafezi, and M. J. Gullans, Fault-tolerant fermionic quantum computing, arXiv preprint arXiv:2411.08955 10.48550/arXiv.2411.08955 (2024).

[23] K. Fukui, T. Matsuura, and N. C. Menicucci, Efficient concatenated bosonic code for additive gaussian noise, Phys. Rev. Lett. **131**, 170603 (2023).

[24] C. Chamberland, K. Noh, P. Arrangoiz-Arriola, E. T. Campbell, C. T. Hann, J. Iverson, H. Putterman, T. C. Bohdanowicz, S. T. Flammia, *et al.*, Building a fault-tolerant quantum computer using concatenated cat codes, PRX Quantum **3**, 010329 (2022).

[25] A. Steane, Multiple-particle interference and quantum error correction, Proc. R. Soc. A **452**, 2551 (1996).

[26] T. Kalajdzievski and J. M. Arrazola, Exact gate decompositions for photonic quantum computing, Phys. Rev. A **99**, 022341 (2019).

[27] D. Su, C. Weedbrook, and K. Brádler, Correcting finite squeezing errors in continuous-variable cluster states, Phys. Rev. A **98**, 042304 (2018).

[28] Y. Liu, S. Singh, K. C. Smith, E. Crane, J. M. Martyn, A. Eickbusch, A. Schuckert, R. D. Li, J. Sinanan-Singh, M. B. Soley, T. Tsunoda, I. L. Chuang, N. Wiebe, and S. M. Girvin, Hybrid oscillator-qubit quantum processors: Instruction set architectures, abstract machine models, and applications, PRX Quantum 10.1103/4rf7-9tfx (2025).

[29] J. i. Yoshikawa, Y. Miwa, A. Huck, U. L. Andersen, P. van Loock, and A. Furusawa, Demonstration of a quantum nondemolition sum gate, Phys. Rev. Lett. **101**, 250501 (2008).

[30] E. Knill and R. Laflamme, Theory of quantum error-correcting codes, Phys. Rev. A **55**, 900 (1997).

[31] S. Lloyd and J.-J. E. Slotine, Analog quantum error correction, Phys. Rev. Lett. **80**, 4088 (1998).

[32] E. T. Hockings, A. C. Doherty, and R. Harper, Scalable noise characterization of syndrome-extraction circuits with averaged circuit eigenvalue sampling, PRX Quantum **6**, 010334 (2025).

[33] D.-G. Welsch, W. Vogel, and T. Opatrný, Homodyne detection and quantum state reconstruction, Prog. Opt. **39**, 63 (1999).

[34] C. González-Arciniegas, P. Nussenzveig, M. Martinelli, and O. Pfister, Cluster states from gaussian states: Essential diagnostic tools for continuous-variable one-way quantum computing, PRX Quantum **2**, 030343 (2021).

[35] B. W. Walshe, B. Q. Baragiola, R. N. Alexander, and N. C. Menicucci, Continuous-variable gate teleportation and bosonic-code error correction, Phys. Rev. A **102**, 062411 (2020).

[36] L. Hu, Y. Ma, W. Cai, X. Mu, Y. Xu, W. Wang, Y. Wu, H. Wang, Y. Song, C. Zou, S. M. Girvin, L.-M. Duan, and L. Sun, Demonstration of quantum error correction and universal gate set on a binomial bosonic logical qubit, Nat. Phys. **15**, 503 (2019).

[37] S. Hao, X. Deng, X. Su, X. Jia, C. Xie, and K. Peng, Gates for one-way quantum computation based on einstein-podolsky-rosen entanglement, Phys. Rev. A **89**, 032311 (2014).

[38] T. Kalajdzievski and N. Quesada, Exact and approximate continuous-variable gate decompositions, Quantum **5**, 394 (2021).

[39] M. Walschaers, Non-gaussian quantum states and where to find them, PRX Quantum **2**, 030204 (2021).

[40] J. Wu and Q. Zhuang, Continuous-variable error correction for general gaussian noises, Phys. Rev. Applied **15**, 034073 (2021).

[41] T. C. Ralph, Quantum error correction of continuous-variable states against gaussian noise, Phys. Rev. A **84**, 022339 (2011).

[42] M. Jiang, T. Wu, J. W. Blanchard, G. Feng, X. Peng, and D. Budker, Experimental benchmarking of quantum control in zero-field nuclear magnetic resonance, Sci. Adv. **4**, eaar6327 (2018).

[43] X. Li, J. Wang, Y.-Y. Jiang, G.-M. Xue, X. Cai, J. Zhou, M. Gong, Z.-F. Liu, S.-Y. Zheng, D.-K. Ma, M. Chen, W.-J. Sun, S. Yang, F. Yan, Y.-R. Jin, S.-P. Zhao, X.-F. Ding, and H.-F. Yu, Cosmic-ray-induced correlated errors in superconducting qubit array, Nat. Commun. **16**, 4677 (2025).

[44] A. Kessy, A. Lewin, and K. Strimmer, Optimal whitening and decorrelation, Am. Stat. **72**, 309 (2018).

[45] R. Schnabel, Squeezed states of light and their applications in laser interferometers, Phys. Rep. **684**, 1 (2017).

[46] J. Conrad, J. Eisert, and F. Arzani, Gottesman-kitaev-preskill codes: A lattice perspective, Quantum **6**, 648 (2022).

[47] G. Huang, A. Beccari, N. J. Engelsen, and T. J. Kippenberg, Room-temperature quantum optomechanics using an ultralow noise cavity, Nature **626**, 512 (2024).

[48] R. J. Epstein, S. Seidelin, D. Leibfried, J. H. Wesenberg, J. J. Bollinger, J. M. Amini, R. B. Blakestad, J. Britton, J. P. Home, D. Lucas, D. Stick, P. K. Ghosh, C. Monroe, and D. J. Wineland, Simplified motional heating rate measurements of trapped ions, Phys. Rev. A **76**, 033411 (2007).

[49] N. Ofek, A. Petrenko, R. Heeres, P. Reinhold, Z. Leghtas, B. Vlastakis, Y. Liu, L. Frunzio, S. M. Girvin, L. Jiang, M. Mirrahimi, M. H. Devoret, and R. J. Schoelkopf, Extending the lifetime of a quantum bit with error correction in superconducting circuits, Nature **536**, 441 (2016).

[50] N. Wang, S. Du, W. Liu, X. Wang, Y. Li, and K. Peng, Long-distance continuous-variable quantum key distribution with entangled states, Phys. Rev. Applied **10**, 064028 (2018).

[51] Y. Lu, A. Maiti, J. W. O. Garmon, S. Ganjam, Y. Zhang, J. Claes, L. Frunzio, S. M. Girvin, and R. J. Schoelkopf, High-fidelity parametric beamsplitting with a parity-protected converter, Nature Communications **14**, 5767 (2023).

[52] Z. Leghtas, S. Touzard, I. M. Pop, A. Kou, B. Vlastakis, A. Petrenko, K. M. Sliwa, A. Narla, S. Shankar, and M. H. Devoret, Confining the state of light to a quantum manifold by engineered two-photon loss, Science **347**, 853 (2015).

[53] C. C. Bultink, B. Tarasinski, N. Haandbæk, S. Poletto, N. Haider, D. J. Michalak, A. Bruno, and L. DiCarlo, General method for extracting the quantum efficiency of dispersive qubit readout in circuit qed, Applied Physics Letters **112**, 092601 (2018).

[54] L. Hänggli and R. König, Oscillator-to-oscillator codes do not have a threshold, IEEE Transactions on Information Theory **68**, 1068 (2022).

[55] P. C. Encinar, A. Agustí, and C. Sabín, Digital quantum simulation of beam splitters and squeezing with ibm quantum computers, Phys. Rev. A **104**, 052609 (2021).